

# Milli-scale AcousTac sensing using soft Helmholtz resonators

Jadesola Aderibigbe<sup>1</sup>, Monica Li<sup>2</sup>, Jungpyo Lee<sup>1</sup>, Hannah S. Stuart<sup>1</sup>

**Abstract**—Acoustic transmission, or sound, can effectively communicate information over distances through various media. We focus on generating acoustic transmission using pneumatically driven resonators for wireless tactile sensing without the need for any electronics at the end-effector or contact point. We explore the relationship between emitted frequency and the geometry of the resonance chamber. When a normal compressive force is applied to the end cap, the compliant resonant cavity deforms, leading to an increase in frequency measurable by an external microphone. Prior work uses tube resonators with fipple attachments. In the present work, we study whether a different smaller audible cylindrical resonator with air blown across the entryway can be utilized instead. We test the utility of the Helmholtz resonator model in predicting the experimental frequency response. Resonance is often modeled for rigid cavities, presenting unique challenges in predicting resonance for the design of soft resonating taxels.

## I. INTRODUCTION

A sense of touch enables dexterity in robot grasping and manipulation [1]. However, practical challenges regarding the fabrication and maintenance of fragile electrical transducers at the contact point limits real-world adoption [2]. Various options have been previously developed to create a physical barrier, or separation, between transducers and the point of contact, such as the GelSight [3] or fluidic innervation [4]. These technologies position cameras or pressure transducers away from the point of contact but still physically link them together and require integration of connecting materials. As a consequence, transducers and contact surfaces cannot be independently maintained, swapped, or replaced. We seek to generate compliant tactile sensors that remove physical integration of electronics from the end-effector altogether. Specifically, we do so by producing sounds that relate to contact state and transmit through the environment.

Prior research utilizes electronic sound emitters and microphones within soft structures [5], [6], showing the utility of sound as a transmission medium in soft robot applications. Yet, the speaker was placed within approximately 0-40 mm of the contact point. Instead of an electronic emitter to produce sound, Li et al. (2022) use constant air flow to drive sound waves in open-closed cavities and generate resonance frequencies sensitive to contact force [7], [8]; variable-length resonance tubes with fipples attached, on the order of 100 mm long, produce a frequency range of 3-5.5 kHz. We seek to reduce the length of the acoustic tactile sensor to less

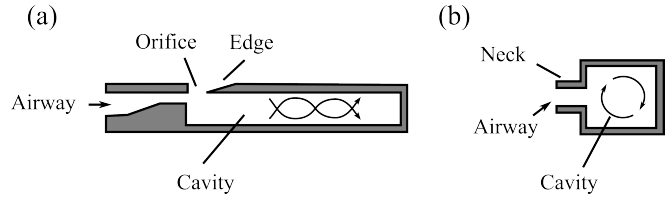


Figure 1: Schematic diagram of two different acoustic resonator geometries: (a) a fipple tube (b) a Helmholtz resonator.

than 1/10th of the initial AcousTac while achieving a similar frequency range. By reducing the length and bulkiness of implementation, resulting taxels can be included in thinner robot appendages.

The current investigation focuses on cylindrical flow-excited Helmholtz resonators, absent of the fipple-tubes used in prior work (Fig. 1).<sup>1</sup> Helmholtz resonators consist of a rigid thin walled cavity with a neck [9]. One example of an everyday Helmholtz resonator is a glass bottle [10]; blowing air across the opening of the bottle leads to sound production from the excitation of the cavity. Chambers of various neck-to-cavity proportions, volumes, and numbers of necks resonate according to the Helmholtz equation which describes emitted frequency, with the addition of correction factors [11]–[13].

We evaluate the frequency response of milli-scale Helmholtz resonators in response to external force as a means to produce a tactile sensor, which we call Milli-scale AcousTac (MAT). Prior work shows that frequency is dependent on the geometry of tube resonator chambers, but still assumes rigid walls. The addition of a compliant cap structure generates a relationship between force, geometry, and frequency detectable with a conventional microphone. In this paper, we introduce MAT for the first time and characterize its force-frequency relationship.

### A. Overview

In Section II we detail the implementation of MAT taxels. We then describe a Helmholtz resonator model from prior work in Section III and propose a fitting procedure for MAT motivated by finite element analysis (FEA) observations. In Section IV, we describe the methods used to measure the force-displacement-frequency response of MAT taxels. The results are reported in Section V. In Section VI, we discuss the robustness of the sensor and acknowledge the intricacies involved in characterizing this soft resonator. In Section VII, we conclude that MAT taxels are a viable

<sup>1</sup> Embodied Dexterity Group, Dept. of Mechanical Engineering, University of California Berkeley, Berkeley, CA, USA.

<sup>2</sup> Dept. of Mechanical Engineering & Materials Science, Yale University, New Haven, CT, USA.

Correspondence to hstuart@berkeley.edu.

<sup>1</sup>The tubes in prior work account for the majority of tactile sensor length.

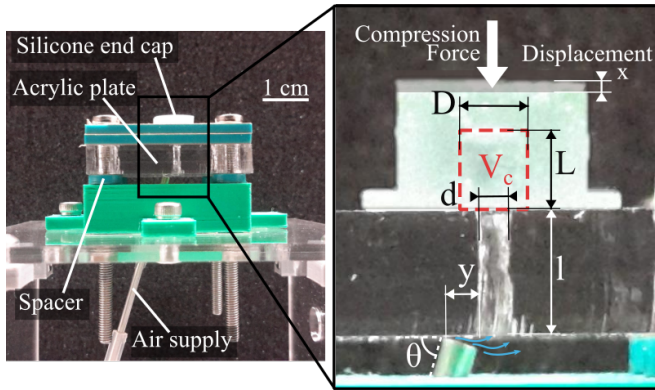


Figure 2: (Left) Close up of taxel components and resonance cavity. (Right) A cross sectional view of the resonant cavity shows how we define compression force and displacement,  $x$ , as well as the dimensions for:  $V_c$ , the upper resonance cavity volume;  $D$  and  $d$ , the diameters of the silicone and acrylic cavities, respectively;  $L$  and  $l$ , the length of the silicone cavity and resonator neck, respectively;  $y$ , the distance between air supply and nearest edge of cavity opening; and,  $\theta$ , the angle of the air supply relative to the plate's surface.

method for producing AcousTac-like signals, at a size scale 10x smaller than prior work.

## II. MAT TAXEL IMPLEMENTATION

The MAT taxel follows the format of a Helmholtz resonator, with a cylindrical cavity attached to a concentric cylindrical orifice of smaller diameter. Fig. 2 depicts a single resonator taxel. The taxel consists of 2 distinct components that connect to form the resonance cavity: a compliant end cap and an acrylic neck. The compliant end cap is cast silicone, Smooth-On Dragon Skin 30 with a circular open-closed channel of radius  $D/2 = 1.59$  mm and length  $L = 4.76$  mm.<sup>2</sup> The acrylic plate is  $l = 6.35$  mm thick with a circular thru-hole – the resonator's neck. The end cap and acrylic plate are mounted to each other using 1.5 mm thick laser cut acrylic guides and dowel pins, then fixed together with bolts. When forces are applied to the end cap, we assume only the silicone portion of the resonator deforms, not the acrylic portion. Both layers, silicone end cap and acrylic plate, are on top an air supply mount with 1.59 mm tall spacers to allow for necessary ventilation. The variation in internal diameter of the compliant end cap versus the acrylic neck in our taxel design is characteristic of a Helmholtz resonator.

The air supply's distance,  $y$ , and angle off the horizontal,  $\theta$ , from the resonance cavity neck opening was selected through a preliminary study. We ran trials with angles ranging from 30 to 75 degrees and distances from 0 to 3.47 mm.<sup>3</sup> Acoustic

<sup>2</sup>Measurements of channel geometry are the dimensions entered into CAD files for laser cutting and specifications from manufacturers. Actual dimensions vary slightly from modelled values based on settings, the ability of a Glow Forge laser cutter and manufacturing tolerances for the dowel pins.

<sup>3</sup>Intervals were not systematically tested, and a working condition was identified simply through trial and error.

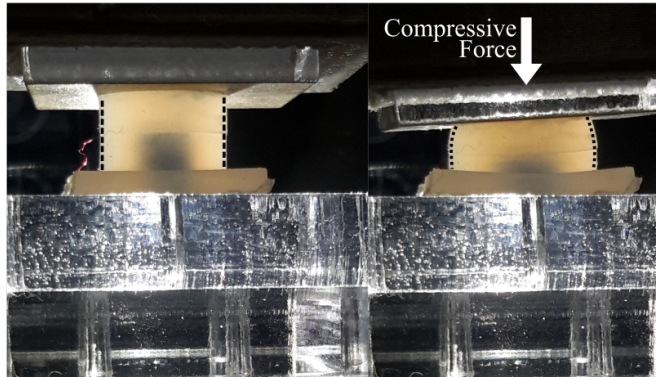


Figure 3: Compression of end cap showing lateral and longitudinal geometry deformation of the end cap

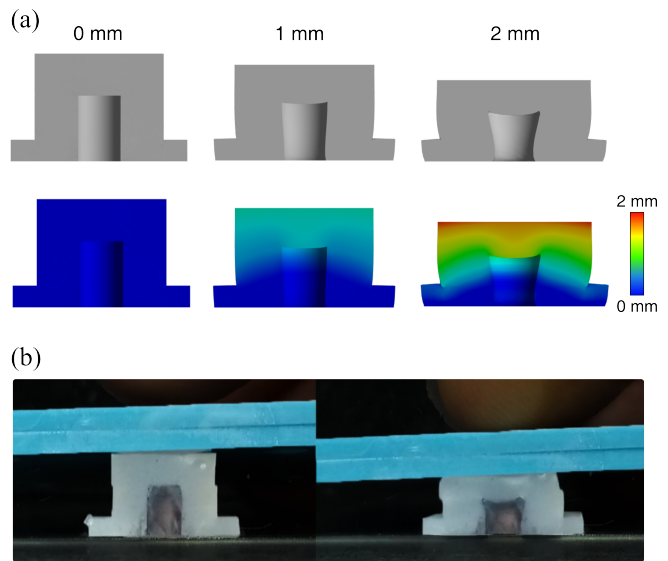


Figure 4: The cross-sectional view of the compliant end cap deformation from (a) FEA simulation and (b) a half-cut end cap. (a) The top row illustrates the geometry of the internal cavity in cross-section for three different deformation stages: 0 mm, 1 mm, and 2 mm of displacement, respectively. The second row represents the corresponding deformation in terms of the displacement distribution, with the color scale indicating the extent of deformation from 0 mm (blue) to 2 mm (red). (b) The geometry of the half-cut end cap from deflection by the manual compression with an acrylic plate.

data was collected at each tested distance and angle combination to find an operable combination for signal clarity and strength (power). We selected  $\theta = 75$  degrees and  $d = 2.10$  mm with a 1.52 mm diameter needle as the air supply to the orifice. We note that the properties and dynamics of the actuating fluid alter frequency response [14]–[16], thus we perform our study with consistent flow conditions.

### A. Taxel deformation

The silicone material used in the study is assumed incompressible and does not result in a 1-to-1 relationship of displacement of the linear stage to changes in the length

of the resonance channel. The compressive loading of the cylindrical end cap results in bulging on the unsupported sides (Fig. 3). We conduct finite element analysis (FEA) to observe the deformation of the internal cavity of the end cap under compression force with Ansys Mechanical Workbench 2024 for deformation stimulation of a hyperelastic material. The 1st order Ogden model is used for Dragon Skin 30 (Smooth-on, USA) silicone [17]. The end cap's base is set to a fixed-support, and a 2 mm displacement is applied on the top of the end cap. The sectional view of the end cap deformation is shown in Fig. 4a. As the displacement increases, the top portion of the cavity begins to bulge inward, pushing towards the interior of the cavity, while the walls near the upper part start to deflect outward. To compare the FEA simulation to the real deflection of the fabricated end cap, we observe a cross-sectional view of the cavity deflection of the end cap (Fig. 4b). As simulated in the FEA environment, the half-cut end cap shows bulging inward at the top portion and widening at the upper portion of the internal walls. Thus, volume change rate is not constant with normal deflection of the end cap, but it decreases as the end cap deflects due to hyperelastic deformation. These observations highlight the complexity and non-linearity of compliant and incompressible silicone under deformation conditions, not captured by an idealized Helmholtz model, which pose a challenge in building a mathematical model of MAT's emitted frequency under load.

### III. MODELLING

At resonance, a volume of fluid in the cavity compresses and expands periodically while fluid at the neck oscillates. This pressure perturbation creates an audible sound. Helmholtz developed a theoretical formula, derived from the wave equation for calculating the resonance frequency of a cavity with circular orifice [18]. Further work from Rayleigh [19] developed additional experimental formula to account for fluid motion outside of the cavity. Adding a length dependent correction factor to the Helmholtz equation to account for the additional fluid motion and abrupt geometry change between the cavity and neck. Ultimately, Rayleigh's Helmholtz equation adds correction factors to the equation to better represent real world environments [20]:

$$f = \frac{c}{2\pi} * \sqrt{\frac{A}{V_c l (1 + c_f \xi)}} \quad (1)$$

where  $c_f$  and  $\xi$  are both geometry based correction factors.

The frequency of the MAT taxel changes depending on the displacement of the end cap due to an external compressive force. Since  $\xi$  and  $c_f$  change as the end cap is compressed, as shown in Fig. 4, we define the effective volume of the cavity,  $V_{c,eff}$ , and our empirical formula for MAT is as follows:

$$f = \left(\frac{c}{2\pi}\right) * \sqrt{\frac{A}{l V_{c,eff}}} \quad (2)$$

We propose a relationship between force and effective volume as

$$V_{c,eff} = V_{c,i} - \alpha F \quad (3)$$

Nomenclature	
$f$	Frequency [1/s]
$d$	Neck channel diameter [mm]
$D$	End cap channel diameter [mm]
$l$	Neck length [mm]
$c$	Speed of sound [m/s]
$c_f$	Correction factor
$\alpha$	Deflection coefficient [mm <sup>3</sup> /N]
$A$	Cross sectional area of neck channel [mm <sup>2</sup> ]
$V_c$	End cap cavity volume [mm <sup>3</sup> ]
$V_{c,i}$	Initial end cap volume [mm <sup>3</sup> ]
$V_{c,eff}$	Effective end cap cavity volume [mm <sup>3</sup> ]
$\xi$	$d/D$
$F$	Compressive Load [N]

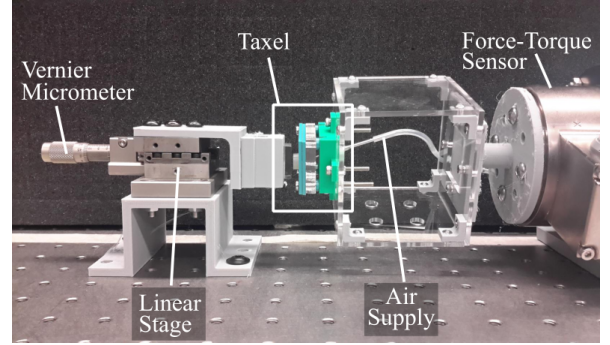


Figure 5: The Newport Linear Stage and SM-13 Vernier Micrometer (left) apply compressive loads through displacement to the taxel (center). As the silicone end cap of the pneumatically driven acoustic taxel compresses, the loads are measured by the ATI force/torque sensor (right).

where  $V_{c,i}$  is an initial volume of the cavity and  $\alpha$  is a deflection coefficient. Assuming deflection and force is linearly related, the volume change rate decreases as the deflection of the end cap increases due to the bulging effect as shown in the FEA result (Fig. 4). Therefore, we can define  $\alpha$  as

$$\alpha = aF + b \quad (4)$$

where  $a < 0$  and  $b$  are dependent on factors such as material stiffness, geometry, etc.

Eq. (3) can be rearranged as

$$f = \frac{c}{2\pi} * \sqrt{\frac{A}{l(V_{c,i} - aF^2 - bF)}} \quad (5)$$

This form of the Helmholtz equation shows that an increase in compressive force results in an increase in frequency of MAT.

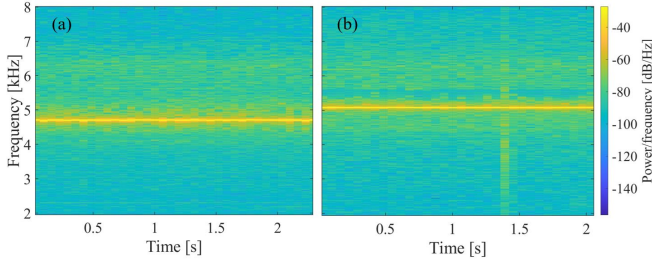


Figure 6: Audiospectrogram of (a) an unloaded taxel and (b) a taxel loaded to 15.4 N and displaced 1.91 mm.

## IV. EXPERIMENTAL METHODS

### A. Instrumentation and setup

Fig. 5 illustrates the horizontal testing configuration. Researchers secured all components to an optical table positioned on a stable surface to minimize unintended motion. An ATI Gamma force/torque sensor attaches to the optical table using a 3D-printed fixture. An adaptor bolts to the force/torque sensor to mount the taxel and air supply tubing. Positioned to the left of the taxel, a Newport SM-13 Vernier Micrometer and linear stage are aligned with the taxel and sensor on the optical table with a PLA mount. This configuration enables static compression of the affixed taxel. A Samsung Galaxy Note 10.1 tablet records sound from approximately 10 cm in front of the testing configuration at a sampling rate of 44.1 kHz.<sup>4</sup> The researchers maintain the flow of wall compressed air through 9.53 mm Dia. tubing and an analog flow meter (1-10 L/min), at around 1.5 L/min before entering a 1.52 mm Dia. tube to excite the resonance cavity of the taxel.

### B. Data acquisition and analysis

By compressing the length of the resonance channel we characterize the relationship between the taxel's displacement, compression, and frequency. We vary the displacement of the compliant taxel, ranging from 0.87 mm to 2.87 mm in increments of 0.50 mm, and measure the resulting force and frequency to characterize this sensor. Note that resonance may not occur at 0 mm, thus two additional points with displacements of 0.05 mm and 0.17 mm are also measured to approximate initial contact state. At each displacement, we record sound and force for about 10 seconds each. We average both the sound and force over the collected time period. We apply a similar method as Li, et al. for acoustic data processing [7]. Using MATLAB's *spectrogram()* and *tfridge()* functions, we extract the resonant frequency from the raw amplitude data (Fig. 6). The power spectrum (*pspectrum()*) of the raw amplitude data finds the peak power and frequency of the acoustic signal within a given working frequency range of 4-5.5 kHz. Using this method, we find root mean square (RMS) error for frequency is negligible, e.g., for the data collected in Fig. 6, RMS error is 1.6 Hz.

<sup>4</sup>Given that sound is measured over narrow frequency bands of  $\sim 500$  Hz in this study, we assume frequency response characteristics of this particular microphone are negligible.

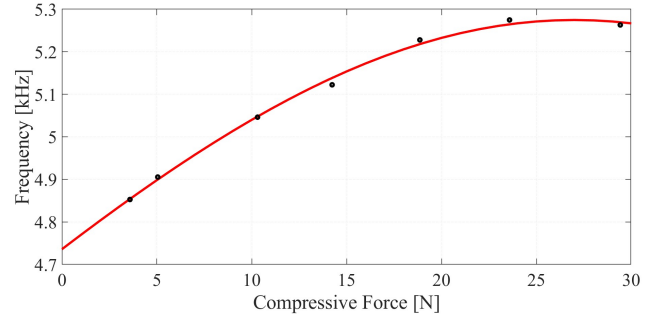


Figure 7: Frequency response to varying force. Experimental force-frequency data, black circles, with the theoretical model fit line from Eq. (5).

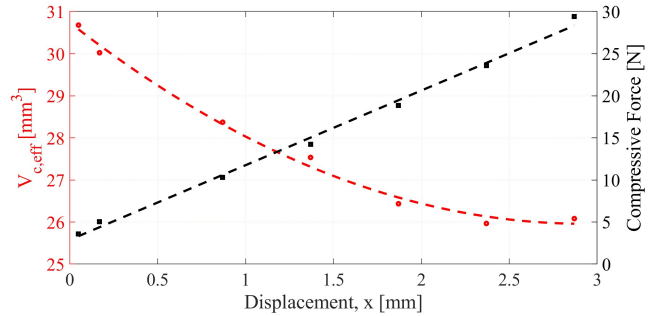


Figure 8: Resonant chamber volume and end cap force in response to varying displacement. Calculated effective cavity volume at specific displacements, red circles, with corresponding linear fit line, red dashed line. Experimental displacement-force data, black squares with corresponding linear fit line, black dashed line. Where  $V_{c,eff} = 0.5576x^2 - 3.2659x + 30.7400$ ;  $F = 8.8719x + 2.8760$ .

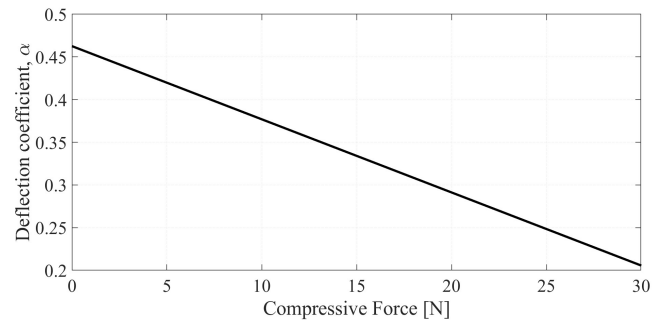


Figure 9: Deflection coefficient,  $\alpha$ , versus compressive force,  $F$ , calculated from Eq. (4).

## V. RESULTS

In the analysis presented, Figs. 7 to 9 provide a comprehensive look at the experimental findings and the validity of the MAT model, Eq. (5). Fig. 7 plots the experimental force-frequency data. We find a monotonic relationship between frequency and force up to approximately 25 N, thus the suggested operating range for this particular taxel. The data align with the trendline generated from the model described in equation Eq. (5). The correlation between the experimental data and the trendline is expected because factors  $V_{c,eff}$  and  $\alpha$  are empirically fit. Yet, the apparent match between the shape of the model and the data supports

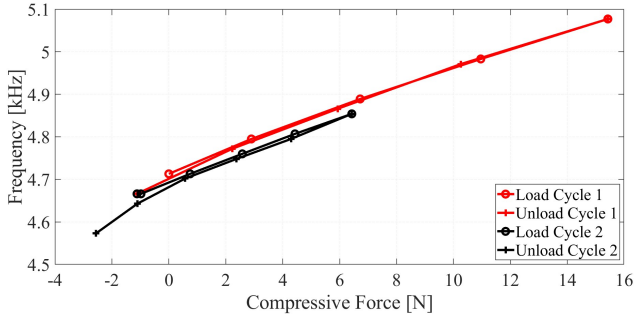


Figure 10: Frequency response of MAT cyclic loading.

our assumptions regarding these factors as a function of force. We report, in Fig. 8, the effective volume against displacement, fit as a second order polynomial consistent with Eq. (3). As displacement increases, the effective volume exhibits a nonlinear reduction; a greater deflection leads to a slower rate of volume change. We confirm a linear relationship between force and displacement under the tested loading conditions. Fig. 9 plots the relationship between the deflection coefficient,  $\alpha$ , and applied force. This relationship incorporates coefficients defined in Eq. (5),  $a = -0.0086$  and  $b = 0.4626$ .

To further evaluate the MAT taxel’s sensing capability, we perform hysteresis analysis using cyclic loading-unloading compression forces, as shown in Fig. 10. We first load and unload the taxel up to 15.4 N (the approximate linear range of the sensor from Fig. 7) and down to -1.1 N. We note that there appears to be an adhesive effect of the taxel when unloading, such that negative tensile forces can be detected after substantial initial compression. This trial demonstrates a one-to-one relationship between force and frequency during both the loading and unloading phases. A second loading cycle occurs up to 6.4 N. Notable variation between the two trials is 24 Hz at 6.4 N, despite relatively small in-cycle hysteresis. This experiment suggests sensor inaccuracy between compressive cycles to be around 1 N. Because low hysteresis is a characteristic that supports accuracy and repeatability of sensor readings in dynamic applications, between cycle variation should be studied further as well as tested across the full sensing range.

## VI. DISCUSSION

The mechanics of the compliant cavity material introduces complexity to design selection and sensor interpretation of MAT. For example, polymers may dampen sound and vibrations in a system [21]. The dynamics of cavity wall vibration may also be influenced by contact state [8]. For example, a measured cavity volume without compressive force is  $37.81 \text{ mm}^3$  and an effective volume calculated by the Eq. (3) is  $32.21 \text{ mm}^3$ . Ideally, those two volumes should be the same. This discrepancy could come from the factors mentioned above. Despite these nonidealities, the results appear to match with trends characteristic of prior Helmholtz resonators.

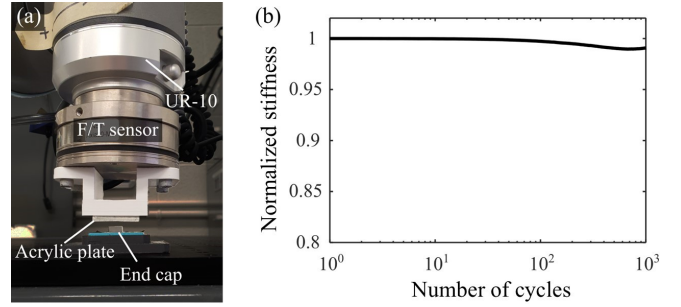


Figure 11: The result from cyclic loads on the silicone end cap. (a) A robotic setup for cycling loads on the end cap. (b) Result of cyclic loads, showing normalized stiffness changes of the end cap over the number of cycles.

### A. Cyclic loads on the end cap

Large strains are unavoidable in soft robotics applications, resulting in limitations in performance due to fatigue and failure after repeated loads on electronic components [2]. Tactile sensors support grasping and manipulation applications, and compliant end effectors made of soft materials offer many advantages, such as mechanical adaptability to objects. Therefore, an electronics-free tactile sensor for soft materials has substantial benefits in contact-rich applications.

To evaluate the mechanical robustness of the electronics-free MAT end cap from repeated loads, we apply cyclic loads to the end cap and monitor how its stiffness changes over multiple cycles. A 2 mm deformation is applied to the top of the end cap with an acrylic plate mounted on a Universal Robot (UR-10) robot arm, and the normal force at 2 mm is measured for 1,000 cycles with a wrist Force Torque (F/T) sensor, as shown in Fig. 11. The result presents that the stiffness of the end cap maintains over 99.1% of its initial value for up to 1,000 cycles. This shows that the proposed MAT can be durable and suitable for applications even under repeated loading conditions compared to traditional transducer-contact-based sensors, which may degrade more quickly. Thus, MAT can reliably perform applications that need repeated loading, such as robotic pick-and-place.

### B. Limitation and future work

The interplay of material properties, geometric variability and flow conditions influences the resonance frequency of soft Helmholtz resonators. The utilization of silicone in the fabrication of soft Helmholtz resonators prompts several considerations regarding manufacturing and modelling frequency. Previous studies demonstrate how damping and structural interactions inherent in silicone can alter frequency response [21]. The casting process for the end cap may also lead to geometric inconsistencies, such as the introduction of micro-bubbles, altering effective stiffness. In this work, we limited our tests to only normal forces, however shear forces may deform the cap as well. Future work that characterizes shear force sensitivity, as it relates to cap geometry, could inform new designs that differentiate loading direction. Researchers must also account for variations in

flow conditions, to which resonance frequency is sensitive. Changes in flow speed can induce “overblowing,” while excitation at higher harmonics may result in the resonator behaving in unpredicted manners. These examples highlight the importance of considering both material properties and environmental factors in the design and application of Helmholtz resonators as tactile sensors. Future studies should vary additional parameters in the MAT taxel design space, such as flow speed, chamber geometries, spacer height, and cap mechanical properties.

Overall scalability of MAT, to both smaller and larger taxels or generating large arrays of MAT taxels, would also reveal further design constraints. As seen in Eq. (1), higher frequencies are achieved by reducing the size of the taxel; future work should characterize the limitations of this down-scaling and whether the frequency can become ultrasonic.

## VII. CONCLUSION

This study introduces a pneumatically driven, electronics-free tactile sensor. By leveraging the unique properties of acoustic wave propagation and soft materials a sensitive and compact (less than 12 mm in length and 10 times smaller than that demonstrated in prior work [7]) taxel emits force information with sound. The experimental results demonstrate that external contact forces influence changes in end cap geometry, producing a measurable effect on the acoustic signal the taxel generates. Therefore, we find that this resonator implementation is feasible for tactile sensing applications. Because this sensor is driven by air flow and measured by conventional microphone, the motivation for this work is to generate a touch-sensing solution that can be integrated into pneumatically driven robots that already have an onboard microphone. By generating physically resilient tactile sensors, more robots can access a sense of touch. Generating resonance that transmits contact information as sound provides one mechanism to do so.

## ACKNOWLEDGMENT

This work of J. Aderibigbe was as supported in part by The GEM Fellowship Program. This work was supported by the Don M. Cunningham Endowed Professorship and by the University of California at Berkeley. The authors acknowledge the support of the members of the Embodied Dexterity Group.

## REFERENCES

- [1] M. R. Cutkosky and W. Provancher, *Force and Tactile Sensing*. Cham: Springer International Publishing, 2016.
- [2] J. Yin, P. Aspinall, V. J. Santos, and J. D. Posner, “Measuring Dynamic Shear Force and Vibration With a Bioinspired Tactile Sensor Skin,” *IEEE Sensors Journal*, vol. 18, no. 9, pp. 3544–3553, 2018.
- [3] W. Yuan, S. Dong, and E. H. Adelson, “Gelsight: High-Resolution Robot Tactile Sensors for Estimating Geometry and Force,” *Sensors*, vol. 17, no. 12, p. 2762, 2017.
- [4] R. L. Truby, L. Chin, A. Zhang, and D. Rus, “Fluidic innervation sensorizes structures from a single build material,” *Science advances*, vol. 8, no. 31, p. eabq4385, 2022.
- [5] G. Zöllner, V. Wall, and O. Brock, “Active Acoustic Contact Sensing for Soft Pneumatic Actuators,” in *2020 IEEE International Conference on Robotics and Automation (ICRA)*. IEEE, 2020, pp. 7966–7972.
- [6] D. S. Drew, M. Devlin, E. Hawkes, and S. Follmer, “Acoustic Communication and Sensing for Inflatable Modular Soft Robots,” in *IEEE Int. Conf. on Robotics and Automation (ICRA)*. IEEE, 2021, pp. 11 827–11 833.
- [7] M. S. Li, T. M. Huh, C. R. Yahnker, and H. S. Stuart, “Resonant Pneumatic Tactile Sensing for Soft Grippers,” *IEEE Robotics and Automation Letters*, vol. 7, no. 4, pp. 10 105–10 111, 2022.
- [8] M. S. Li and H. S. Stuart, “Acoustac: Tactile sensing with acoustic resonance for electronics-free soft skin,” *Soft Robotics*, 2024.
- [9] L. Rayleigh, “The theory of the Helmholtz resonator,” *Proc. of the Royal Society of London. Series A*, vol. 92, no. 638, pp. 265–275, 1916.
- [10] A. Cummings, “Acoustics of a cider bottle,” *Applied Acoustics*, vol. 5, no. 3, pp. 161–170, 1972.
- [11] S. Tang, “On Helmholtz resonators with tapered necks,” *Journal of Sound and Vibration*, vol. 279, no. 3, pp. 1085–1096, 2005.
- [12] A. Selamet and I. Lee, “Helmholtz resonator with extended neck,” *The Journal of the Acoustical Society of America*, vol. 113, no. 4, pp. 1975–1985, 2003.
- [13] N. M. Papadakis and G. E. Stavroulakis, “FEM Investigation of a Multi-Neck Helmholtz Resonator,” *Applied Sciences*, vol. 13, no. 19, p. 10610, 2023.
- [14] P. Nelson, N. Halliwell, and P. Doak, “Fluid dynamics of a flow excited resonance, Part II: Flow acoustic interaction,” *Journal of Sound and Vibration*, vol. 91, no. 3, pp. 375–402, 1983.
- [15] F. Ghanadi, M. Arjomandi, B. Cazzolato, and A. Zander, “Interaction of a flow-excited Helmholtz resonator with a grazing turbulent boundary layer,” *Experimental thermal and fluid science*, vol. 58, pp. 80–92, 2014.
- [16] S. N. Njane, Y. Shinohara, N. Kondo, Y. Ogawa, T. Suzuki, and T. Nishizu, “Improved underwater Helmholtz resonator with an open cavity for sample volume estimation,” *Computers and Electronics in Agriculture*, vol. 147, pp. 18–26, 2018.
- [17] M. Elkeran, M. Fanni, and H. Iwata, “Material modeling and development of soft surgical robots using transient finite element analysis,” *Int. J. Mech. Mechatronics Eng*, vol. 20, pp. 25–34, 2020.
- [18] H. v. Helmholtz, “Theorie der Luftschwingungen in Röhren mit offenen enden.” 1860.
- [19] J. W. S. B. Rayleigh, *The Theory of Sound*. Macmillan, 1896, vol. 2.
- [20] G. Catapane, D. Magliacano, G. Petrone, A. Casaburo, F. Franco, and S. De Rosa, “Semi-analytical estimation of Helmholtz resonators’ tuning frequency for scalable neck-cavity geometric couplings,” *CEAS Aeronautical Journal*, vol. 13, no. 3, pp. 797–808, 2022.
- [21] V. Geethamma, R. Asaletha, N. Kalarikkal, and S. Thomas, “Vibration and sound damping in polymers,” *Resonance*, vol. 19, pp. 821–833, 2014.